

Ion core effect on transport characteristics in warm dense matter

T.S. Ramazanov, M. Issanova, Ye.K. Aldakul, and S.K. Kodanova*

Institute for Experimental and Theoretical Physics, Al-Farabi Kazakh National University, 71 Al-Farabi ave., 050040 Almaty, Kazakhstan

An effective potential approach in combination with the molecular dynamics (MD) method was used to study the effect of the ionic core on the transport properties of ions in the warm dense matter regime. As an example, we considered shocked silicon. The results of MD simulations within microcanonical ensemble were analyzed by computing the mean squared displacement (MSD) and the velocity autocorrelation function (VAF) of particles. The MSD and VAF are used to compute the diffusion coefficient of ions. The results are compared with the data computed neglecting the ion core effect. It is found that the ion core effect leads to a significant decrease of the diffusion coefficient. Additionally, we computed the viscosity coefficient of ions using the Green-Kubo relation connecting viscosity and the stress autocorrelation function. It is revealed that the ion core effect can cause increase or reduction of the viscosity coefficient depending on the strength of inter-ionic coupling.

I. INTRODUCTION

An interest in warm dense matter (WDM), a state with high temperature and density, is fueled due to development of new facilities where extreme conditions are created by laser driven heating and shock compression (e.g. see Refs. [1, 2] for the discussion of relevant system parameters). These experiments are motivated by the fact that WDM is found in various astrophysical objects, such as giant planets [3–5], white and brown dwarfs [3, 6], and interiors of stars [7]. Additionally, warm dense plasma is generated in experiments on inertial thermonuclear fusion [8]. An example of experimental discovery that have been made in this field is diamond formation due to irradiation of material surfaces with intense plasma flows, etc. [9, 10]. However, a comprehensive understanding of fundamental physical properties of WDM is often hindered by complexity of the required simulations [11–14]. Particularly, the study of the transport properties of ions is challenging due to required long simulation times, e.g. compared to the calculation of structural properties. One possible way to overcome this difficulty is to use an effective potential, extracted from ab initio density functional theory based simulations [15–19] or derived using density response function of electrons [20–28], in molecular dynamics [15, 29].

The computation of transport properties of WDM and dense plasmas is of relevance for practical applications such as inertial confinement fusion [30, 31]. Thus, various approaches were used to compute different transport coefficients in WDM regime, e.g. see the recent review by Grabowski et al [32]. To further deepen our understanding of the physics of transport phenomena at WDM parameters, in this work we perform study of the viscosity and diffusion coefficients in the WDM of shocked silicon. Moreover, for the first time, to our knowledge, we provide an analysis of a transition from ballistic-type diffusion on short time scales to normal diffusion on long time scales taking into account the ion core effect. To capture relevant physical effects, we use the effective potential from Ref. [15], which provides adequate description of structural and

dynamical properties of shocked silicon at WDM conditions. The effective potential is used to model ions by the molecular dynamics (MD) method in the microcanonical ensemble. The latter point is important since it allows us to avoid possible artificial effects due to nonphysical forces in often used schemes with thermostat such as Langevin dynamics and Nosé-Hoover dynamics.

Following Ref. [15], the effective ion-ion potential used in this work reads

$$V(r) = \frac{Z_i^2 e^2}{4\pi\epsilon_0 r} \exp(-k_s r) + \frac{(Z_n^2 - Z_i^2) e^2}{4\pi\epsilon_0 r} \exp[-(b + k_s) r], \quad (1)$$

here Z_i denotes the ion charge state, k_s is the inverse screening length, Z_n is the nuclear charge, and parameter b determines the range of the short-range repulsion. From Eq. (1) one can see that the effective ion-ion interaction is represented by Yukawa type potential with additional short-range repulsion (Yukawa+SRR).

In Eq.(1), the first term is often referred as the Yukawa potential and takes into account the screening of ion-ion interaction in the long-wavelength limit. The second term in Eq.(1) accounts for the bound core electrons and represents what we call the ion core effect in this work.

The aim of this work is the investigation of the ion core effect on the self diffusion process and viscosity at characteristic WDM parameters. To study the diffusion process and compute diffusion coefficient we analyzed the mean squared displacement and velocity auto-correlation function of ions. The latter is used to compute diffusion coefficient using Einstein's relation. The correctness of the value of the diffusion coefficient computed this way is validated by comparing to the data for the diffusion coefficient extracted from the mean squared displacement of ions on long time scales. The viscosity coefficient is computed using the Green-Kubo relation connecting viscosity coefficient and the microscopic stress tensor.

The paper is organized as the following: In the next section II we provide information about used simulation parameters. Then in Sec. III, the results of the MD simulations based on the effective potential (1) are presented. The paper is concluded by summarizing our main findings.

* kodanova@physics.kz

II. SIMULATION PARAMETERS

We took the system parameters as in Ref. [15], i.e. electron density $n_e = 5.36 \times 10^{23} \text{ cm}^{-3}$ and temperature $T_e = 54540 \text{ K}$, $Z_n = 14$, $Z_i = 4$, and mean inter-particle distance $a = (3/4\pi n_i)^{1/3} = 2.291 a_0$, where a_0 is the Bohr radius and n_i is the ion density. We set $b = 0.7 a_0^{-1}$ and $k_s = 1.277 a_0^{-1}$. From latter we obtain the value for screening parameter $\kappa = k_s a = 2.926$. The system temperature is controlled by coupling parameter $\Gamma = Z_i^2 e^2 / 4\pi\epsilon_0 a k_B T_i$, where T_i is the temperature of ions. At $T_i = T_e$, we have $\Gamma = 40.4$. Since WDM state with different temperatures of ions and electrons (i.e. non-isothermal state) is often generated in experiments [33], where ions can be hotter or colder than electrons depending on the way of generation of WDM, we additionally considered different Γ values from 1 to 100. These correspond to ion temperatures in the range between 1.9 eV and 188 eV. This serves our objective which is the elucidation of the ion core effect on transport properties in different ionic correlation regimes.

The investigation was conducted by means of MD simulations. The dynamics of $N = 103823$ identical particles was obtained by solving the equation of motion through Beeman's algorithm with a time step of $t = 0.01\omega_p^{-1}$. We employed periodic boundary conditions with a main box of side length $L = (4\pi N/3)^{1/3}a$. The results are presented in dimensionless units; dimensions of length are reduced by a and a time unit is represented by the inverse plasma frequency of ions ω_p^{-1} . The results from MD simulations are measured within the microcanonical ensemble. This allows us to avoid possible nonphysical effects due to the use of thermostat which, for example, is represented by an additional artificial friction force and compensating it randomly fluctuating force in the case of the Langevin dynamics. We note that such methods like the Langevin dynamics and the Nosé-Hoover dynamics allow one to generate correct ionic configurations within the canonical ensemble, but the transport and dynamic properties can be incorrect since they dependent on actual evaluation of particles trajectories in time.

III. MD SIMULATION RESULTS

A. Radial distribution function

To have better understanding of the results obtained for various considered properties, we calculated the radial distribution function (RDF). The RDFs for a range of coupling parameters are shown in Fig. 1. From Fig. 1 we see that at $\Gamma = 1$ the system shows no significant order in the structure besides of a correlation hole. With increasing value of Γ the RDF shows the emergence of a short-range order, which is indicated by the distinct peaks in the RDF. In Fig. 1, the vertical dashed line at $r/a = 1.42$ represents a characteristic range of the short-range repulsion defined by b^{-1} . At all considered Γ values, there is a significant probability of positioning ions at a distance within range b^{-1} . Thus, we can expect that the

ion core effect is important for transport characteristics at all considered Γ values.

B. Diffusion characteristics

To analyze the effect of an additional repulsion due to ionic core on the diffusion coefficient, we computed the mean squared displacement (MSD) of ions and the velocity auto-correlation function (VACF) of ions. To cover both short- and long-time correlations with a desired accuracy at a minimum computational effort we implemented the modification of the order- n algorithm [34] for computing correlation functions, originally proposed by Frenkel and Smit [35]. The gain in computational effort is possible due to the use of a variable sampling frequency, i.e. short- and long-time correlations are calculated at different sampling frequencies. Implementing a conventional method with the fixed-frequency sampling [35, 36] is impractical as the number of particles gets larger as the desired correlation times become longer.

In most cases the MSD and VACF of a single MD run contain a large statistical noise. To reduce the undesired statistical noise one usually runs several independent MD simulations under the same set of parameters and take the average of the results. Thus, to reduce the statistical noise, the results of the MSD and VACF presented in this paper have been averaged over five MD runs.

We note that the MSD and VACF contain information about microscopic dynamics of particles. The MSD represents how a particle is displaced [in a random direction] from a given position at a given arbitrary moment in time. In general, the MSD contains more information than the diffusion coefficient, see e.g. Ref. [37]. Information about the diffusion coefficient is extracted from the MSD by analyzing its behavior at long times, which is relevant, e.g., for hydrodynamics. Similarly, in addition to the diffusion coefficient, the VACF contains information about wavenumber-averaged oscillation (excitation) modes [38].

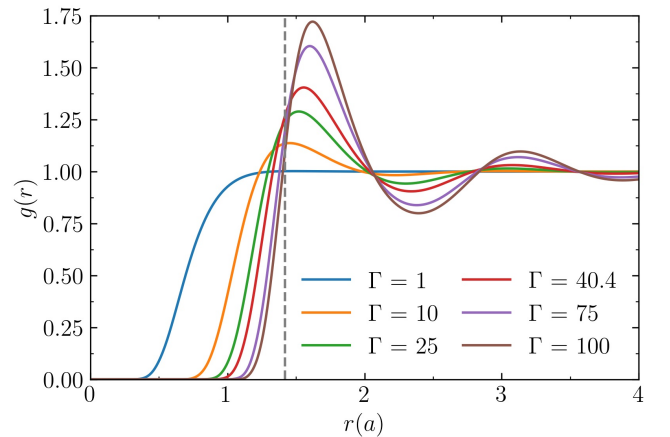


FIG. 1. Radial distribution function of ions computed using Eq. (1) at different coupling parameters.

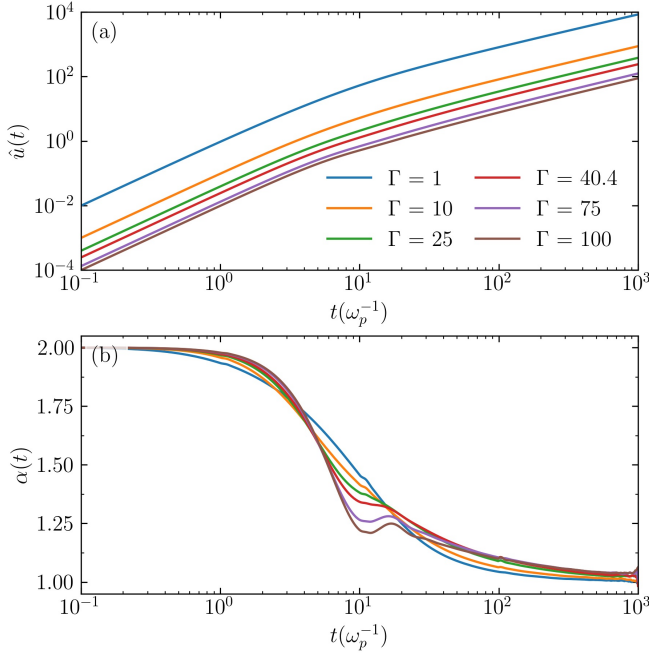


FIG. 2. (a) Reduced Mean Squared Displacement (MSD) of ions with the bound core electrons at different coupling parameter values. (b) Diffusion parameter $\alpha(t)$ of a system of ions as defined by Eq. (3), where α is dimensionless quantity.

The MSD is calculated using the following equation:

$$u(t) = \langle |\mathbf{r}(t) - \mathbf{r}(0)|^2 \rangle, \quad (2)$$

where $\langle \dots \rangle$ denotes ensemble average.

The results of simulations for different values of Γ are presented in Fig. 2. From Fig. 2 we see that, as one would expect, the emergence of order in the system due to the increase of the coupling parameter causes the MSD of particles to decrease. Indeed, at larger Γ values, ions become more confined by neighboring particles and the displacement process becomes less intensive.

In the case of normal diffusion, the MSD must be a linear function of time $u(t) \propto t$. From Fig. 2 (a) one can see that it is the case at long times $t > 100\omega_p^{-1}$. At shorter times the deviation from normal diffusion takes place. For an accurate calculation of the diffusion coefficient, the MSD values should be used at times scales where the normal diffusion regime is well established. For this propose, the deviation from normal diffusion can be analyzed by considering an effective time dependent diffusion parameter α as it is defined through the proportionality

$$u(t) \propto t^\alpha. \quad (3)$$

Fig. 2 (b) shows the diffusion parameter obtained from the analysis of the MSD data presented in Fig. 2 (a). The plot of the diffusion parameter shows that the initial stage of the motion is ballistic, $\alpha = 2$, from which it switches to the intermediate so-called anomalous diffusion, $\alpha \neq 1$, and then converges to the normal diffusion, $\alpha = 1$. We also observe that

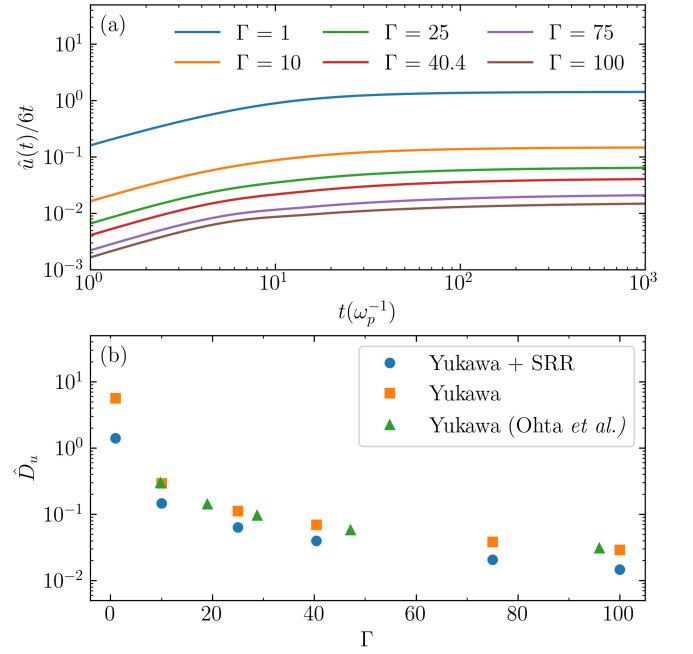


FIG. 3. (a) The ratio $\hat{u}(t)/6t$ as a function of time which shows convergence to a diffusion coefficient, where $u(t)$ is the MSD in units of the square of the mean interparticle distance, a^2 , and t is in units of the inverse ion plasma frequency. (b) The diffusion coefficient values (in units of $\omega_p a^2$) calculated by the Einstein's relation using the Yukawa+SRR potential, Eq. (1), and the standard Yukawa potential. The comparison with the results for Yukawa systems reported by Ohta et al. [39] is also shown.

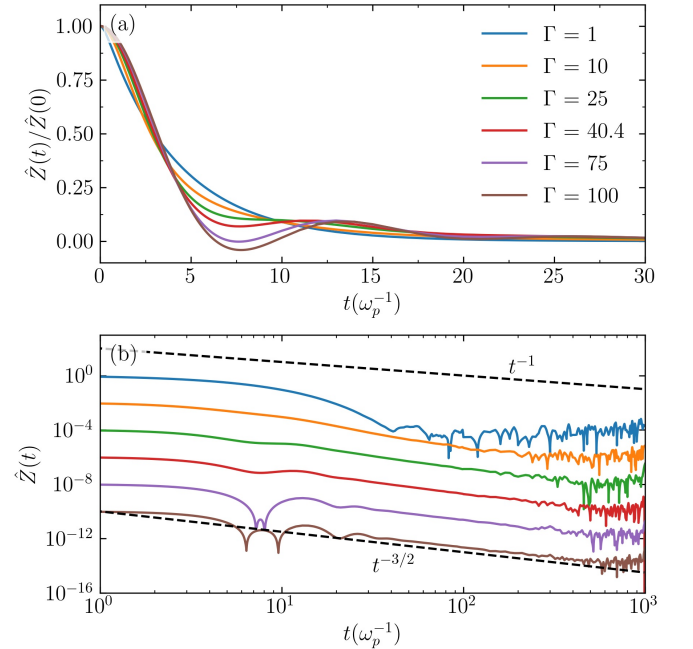


FIG. 4. (a) Velocity autocorrelation function (VACF) of ions at different values of the coupling parameter. (b) The reduced VACF in logarithmic scale where dashed line represents t^{-1} decay. In the subplot (b), the curves of the VACF at $\Gamma > 1$ are shifted down for better visualisation of the behavior at long times.

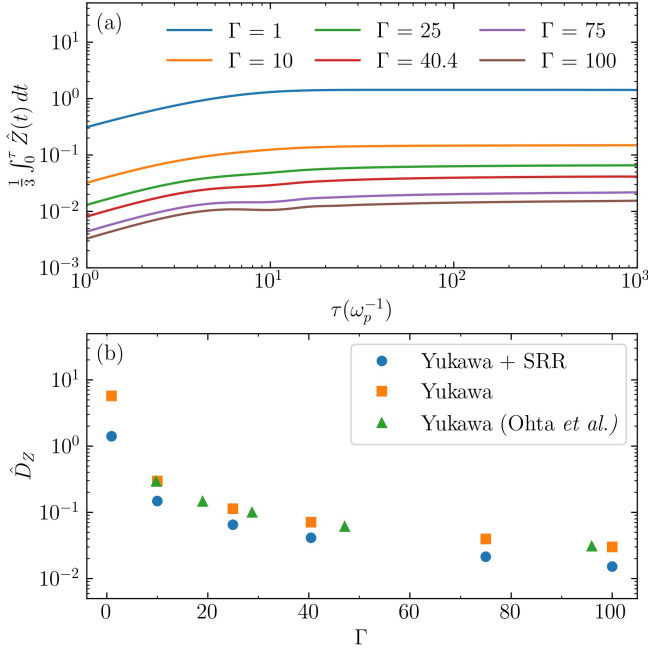


FIG. 5. (a) The VACF integral as a function of time, which shows convergence as the upper limit of integration increases. (b) The diffusion coefficient values (in units of $\omega_p a^2$) calculated by using the Green-Kubo relation on the basis of the Yukawa+SRR potential, Eq. (1), and the standard Yukawa potential. The comparison with the results for Yukawa systems reported by Ohta *et al.* [39] is also shown.

an intermediate diffusion type and the rate of convergence to the normal diffusion are controlled by the value of coupling parameter, the increase in the coupling parameter hinders the convergence to a normal diffusion. Clearly, for capturing a normal diffusion regime in the case of strongly coupled ions characteristic for WDM, one needs to perform measurements at times scales $t \gg 100 \omega_p^{-1}$, where ω_p^{-1} is the plasma period of ions. We note that this represents a significant challenge for a standard Kohn-Sham density functional theory based MD simulations, where computation time of electronic structure at each MD step at considered high temperatures represents a major bottleneck. This is an example where alternative simulation techniques of ions dynamics such as effective potential approach or orbital free density functional method are indispensable.

Next, at long time scales, the values of the diffusion coefficients can be obtained using Einstein's relation:

$$D_u = \lim_{t \rightarrow \infty} \frac{u(t)}{6t}. \quad (4)$$

Fig. 3 (a) shows the ratio $\hat{u}(t)/6t$. From Fig. 3 (a) we see that $\hat{u}(t)/6t$ approaches to a constant value at $t \gg 10^2 \omega_p^{-1}$. However, as it can be seen from Fig. 2 (b), we could not reach exactly normal diffusion regime with $\alpha \equiv 1$ for $\Gamma > 1$. Thus, there is certain error in the diffusion coefficient values computed using Eq. (4). Using Eq. (4) and the average of $u(t)/6t$ in the time interval $500 < t\omega_p < 1000$, we have calculated the approximate values of the diffusion coefficients

summarized in Table I.

The decrease of the diffusion coefficient values with increasing coupling parameter at $\Gamma > 1$ is caused by the emerging local order and caging of an ion by surrounding particles. From Table I we observe that the ion core effect leads to significantly lower values of the diffusion coefficient. This can be understood as the result of stronger inter-particle correlations and stronger caging of an ion by its surrounding.

As mentioned, an error in the calculation of the diffusion coefficient is caused by the deviation of the MSD from the linear dependence on time. In order to cross check the accuracy of our calculations, we used the VACF and the related Green-Kubo equation to computed the diffusion coefficient of ions.

The VACF is a measure of the correlation degree in the velocity of a particle at different times and is defined as:

$$Z(t) = \langle \mathbf{v}(t) \cdot \mathbf{v}(0) \rangle. \quad (5)$$

The results for the VACF of ions at different values of the coupling parameter are shown in the top panel of Fig. 4. At $\Gamma = 1$, the VACF decays monotonically with time. This behavior changes with the increase in Γ and we observe appearance of oscillatory pattern. The diffusion coefficient can be calculated by integrating the VACF over time. This is known as a Green-Kubo relation, which reads:

$$D_Z = \frac{1}{3} \int_0^\infty Z(t) dt, \quad (6)$$

where we introduced notation D_Z in order to distinguish it from the diffusion coefficient D_u computed using the MSD.

To find accurate data for the diffusion coefficient, the integral in Eq. (6) must converge well. In the bottom panel of Fig. 4 we show the VACF using logarithmic scale to better illustrate the behavior of the VACF at long times. At all considered Γ values, the tail of the VACF decays faster than t^{-1} which ensures the convergence of the integral in Eq. (6). However, one can observe from Fig. 4 (b) that the increase in Γ leads to a slower decay of the VACF values at long times. For example, at $\Gamma = 100$, the VACF decays as $t^{-1.5}$ at long times as it is illustrated in Fig. 4 (b). At $\Gamma \geq 10$, one need to generate data at times $t \gg 10^2 \omega_p$. As time increases, significant data fluctuations appear at some point due to a finite number of particles in the MD simulations. Thus, for the calculation of the diffusion coefficient, it is important that these fluctuations begin after the VACF value is sufficiently reduced so that they do not affect the integration accuracy in Eq. (6).

Due to the use of large number of ions in the main cell in our simulations, the convergence of the integral $\int_0^\tau Z(t) dt$ is not affected by fluctuations as it is demonstrated in Fig. 3 (c). The results for the diffusion coefficient D_Z computed using (6) are summarized in Table I, where we again compare with the results computed using the Yukawa potential. From this figure we see the same behavior of the diffusion coefficient D_Z as that of D_u . Table I summarizes the diffusion coefficients calculated by Einstein's and Green-Kubo relations. From this table we see that computed D_Z and D_u values are in agreement

TABLE I. Diffusion coefficients of a system of ions with interaction potential (1) and pure Yukawa potential. Einstein's and Green-Kubo relations are used to calculate the diffusion coefficients from MSD and VACF data, respectively. Error bounds correspond to 95% confidence interval.

Γ	$D_u/\omega_p a^2$	$D_u^{\text{Yukawa}}/\omega_p a^2$	$D_Z/\omega_p a^2$	$D_Z^{\text{Yukawa}}/\omega_p a^2$
1	1.409 ± 0.003	5.62 ± 0.06	1.412 ± 0.005	5.7577 ± 0.007
10	0.1455 ± 0.0008	0.294 ± 0.002	0.1475 ± 0.0007	0.2973 ± 0.001
25	0.0633 ± 0.0006	0.1121 ± 0.0008	0.0649 ± 0.0003	0.1142 ± 0.0002
40.4	0.0399 ± 0.0005	0.0697 ± 0.0007	0.0411 ± 0.0001	0.0713 ± 0.0002
75	0.0206 ± 0.0003	0.0385 ± 0.0005	0.0214 ± 0.0002	0.0399 ± 0.0002
100	0.0146 ± 0.0002	0.0289 ± 0.0005	0.0152 ± 0.0002	0.0302 ± 0.0003

within evaluated statistical uncertainty. The disagreement between D_Z and D_u is about 1% at $\Gamma = 1$ and $\Gamma = 10$, about 2% at $\Gamma = 25$ and $\Gamma = 40.4$, and about 4% at $\Gamma = 75$ and $\Gamma = 100$.

C. Simulation results for viscosity

For the calculation of the viscosity coefficient, we use the Green-Kubo relation connecting viscosity and stress autocorrelation function (SAF):

$$\eta = \frac{1}{k_B T V} \int_0^\infty H(t) dt, \quad (7)$$

where in order to improve statistics, for the SAF we use:

$$H(t) = (H^{xy} + H^{yz} + H^{zx})/3, \quad (8)$$

as the x , y , and z directions are equivalent [40].

For example, zx component of the SAF is defined as

$$H^{zx}(t) = \langle \sigma^{zx}(t) \sigma^{zx}(0) \rangle, \quad (9)$$

with σ^{zx} being the zx component of the microscopic stress tensor:

$$\sigma^{zx}(t) = \sum_{i=1}^N \left[m v_{i,z} v_{i,x} - \frac{1}{2} \sum_{j=1 \neq i}^N \frac{z_{ij} x_{ij}}{r_{ij}} V'(r_{ij}) \right]. \quad (10)$$

The xy and yz components of the SAF and corresponding microscopic stress tensors are defined in a similar way.

During MD simulations, we computed the dynamics of 103823 particles after equilibration for a total time of $10^3 \omega_p^{-1}$. Further, the presented results are averaged over five MD runs.

The results of the computations are presented in Fig. 4. The Fig. 4 (a) shows the SAF for different coupling parameters. From this figure we observe that one needs a high quality data for the SAF at least up to $10\omega_p^{-1}$ for the evaluation of the viscosity using Eq. (7). At considered simulation parameters, nonphysical fluctuations in the data for the SAF become dominant at $t \gtrsim 20\omega_p^{-1}$. However, these fluctuations do not lead to a significant deterioration of the accuracy of the integration in Eq. (7). This can be seen in Fig. 4 (b), where the values of the integral $\int_0^t H(\tau) d\tau$ are shown for different values

TABLE II. Viscosity of a system of ions with interaction potential (1) and pure Yukawa potential. The Green-Kubo relation was used to calculate the viscosity from SACF data. Error bounds correspond to 95% confidence interval.

Γ	$\eta/n_i m_i \omega_p a^2$	$\eta^{\text{Yukawa}}/n_i m_i \omega_p a^2$
1	0.94 ± 0.09	3.5 ± 0.3
10	0.127 ± 0.005	0.24 ± 0.05
25	0.087 ± 0.01	0.081 ± 0.006
40.4	0.076 ± 0.007	0.066 ± 0.007
75	0.074 ± 0.004	0.046 ± 0.004
100	0.071 ± 0.01	0.0358 ± 0.006

of the upper integration limit t . From Fig. 4 (b) we see that the integral $\int_0^t H(\tau) d\tau$ is converged at $t \simeq 20\omega_p^{-1}$ and further increase of the upper integration limit t leads to certain oscillations around a mean value due to aforementioned pure statistics at long times. A maximum value of the amplitude of these oscillations is used to evaluate uncertainty in our data for the viscosity coefficient.

The results for the viscosity coefficient are summarized in Table II and compared with the data obtained for the Yukawa system. At considered values of the coupling parameter, the viscosity decreases with an increase in Γ . From the comparison with the data computed using the Yukawa potential, we see that at relatively small values of the coupling parameter $\Gamma < 25$, the ion core effect leads to a decrease in the viscosity value. In contrast, at large values of the coupling parameter, the ion core effect leads to an increase in the viscosity value. This can be understood considering different terms in Eq. (7). As it is known [41], at relatively small values of Γ , the contribution coming from the term $m v_{i,z} v_{i,x}$ in the summation in Eq. (7) (a kinetic part) is dominant over the contribution due to term $\sum z_{ij} x_{ij}/r_{ij} V'(r_{ij})$ (a correlation part). In contrast, at large Γ values, the correlation part is dominant over the kinetic part in Eq. (7). At $\Gamma < 25$, a stronger ion-ion correlation due to the ion core effect leads to a reduction of the mobility of ions and, thus, reduction of the kinetic part of Eq. (7). As the result, the ion core effect leads to a decrease in the viscosity value. At $\Gamma > 25$, the ion core effect induced stronger ion-ion correlation results in an increase in the correlation part in Eq. (7). Thus, at large values of Γ , the ion core effect causes an increase in the viscosity value.

The presented data Table II have uncertainty in the range from about 5% up to about 14% depending on the coupling

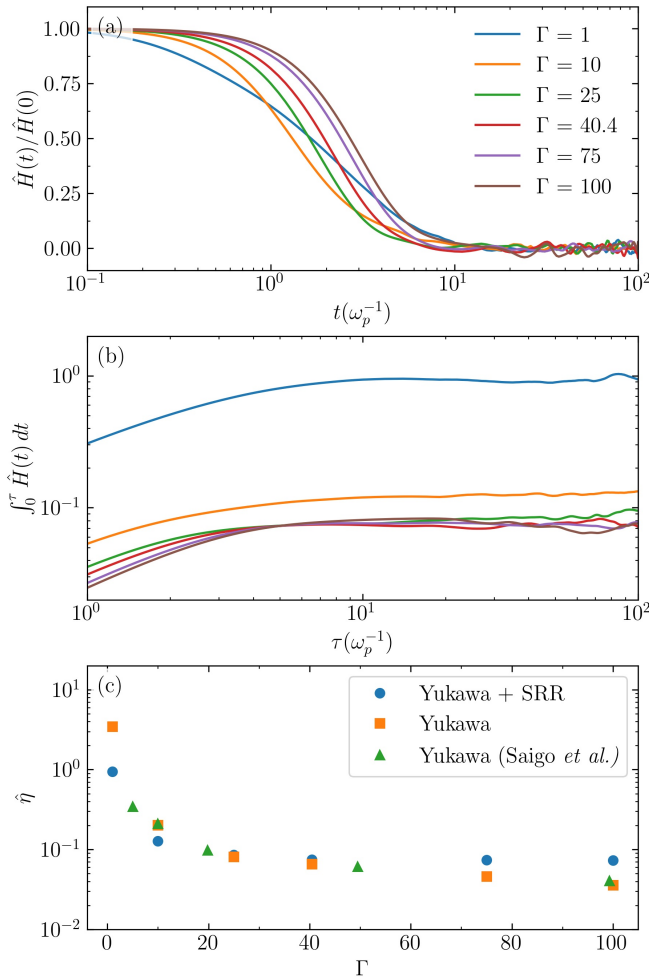


FIG. 6. (a) The stress autocorrelation function (SACF) of ions at different values of the coupling parameter. (b) The integral of the reduced SACF as a function of time, which shows convergence as the upper limit of integration increases. (c) The viscosity values (in units of $n_i m_i \omega_p a^2$ with m_i being the ion mass) calculated by using the Green-Kubo relation, Eq. (7), on the basis of the Yukawa+SRR potential, Eq. (1), and the standard Yukawa potential. The data is compared with the results for Yukawa systems reported by Saigo *et al.* [40].

parameter. Although it is less accurate than the data obtained for the diffusion coefficient in this work, the uncertainty of

the computed values of the viscosity still allows us to clearly distinguish the change in the general trend caused by the ion core effect when compared to the results obtained using the Yukawa potential.

IV. CONCLUSION

In this work we have analyzed the effect of the ion core on the diffusion and viscosity of ions in the WDM. We used the effective ion-ion interaction potential designed to describe the dynamic and static properties of shocked silicon. For the calculation of the diffusion coefficient we used two different approaches. First of all, we used the MSD of ions to compute the diffusion coefficient at long time scales. Additionally, we used the VACF of ions to find the diffusion coefficient employing the Green-Kubo relation connecting the VACF with the diffusion coefficient. These two methods allowed us to crosscheck our results for the diffusion coefficient. It was found that the ion core effect leads to a significant decrease of the diffusion coefficient at $1 < \Gamma \leq 100$. This is in agreement with previously reported observations, e.g. from simulations using an orbital-free density functional theory at the Thomas-Fermi-Dirac level [42]. Similar analysis of the viscosity coefficient computed using corresponding Green-Kubo relation shows that the ion core effect leads to the reduction of viscosity at $\Gamma < 25$ and to the increase of the viscosity at $25 < \Gamma \leq 100$.

The performed analysis of the MD simulations results contributes to our understanding of the transport properties of the WDM. Moreover, it demonstrates the need of large scale MD simulations for an accurate calculation of transport properties of non-ideal ions in the WDM regime and, thus, highlights the need of fast MD simulation methods for further theoretical analysis of the WDM.

ACKNOWLEDGMENTS

This research is funded by the Science Committee of the Ministry of Education and Science of the Republic of Kazakhstan Grant AP08856650 "Study of the structural, transport, and thermodynamic properties of non-ideal multicomponent dense plasma with heavy ions".

[1] M. S. Murillo, Phys. Rev. E **81**, 036403 (2010).
[2] M. Bonitz, T. Dornheim, Z. A. Moldabekov, S. Zhang, P. Hamann, H. Kählert, A. Filinov, K. Ramakrishna, and J. Vorberger, Physics of Plasmas **27**, 042710 (2020).
[3] D. Saumon, W. Hubbard, G. Chabrier, and H. V. Horn, Astrophys. J. **391**, 827 (1992).
[4] B. Militzer, W. Hubbard, J. Vorberger, I. Tamblyn, and S. Bonev, Astrophys. J. **688**, L45 (2008).
[5] T. Guillot, Y. Miguel, B. Militzer, W. Hubbard, Y. Kaspi, E. Galanti, H. Cao, R. Helled, S. Wahl, L. Iess, W. Folkner,

D. Stevenson, J. Lunine, D. Reese, A. Biekman, M. Parisi, D. Durante, J. Connerney, S. Levin, and S. Bolton, Nature (London) **555**, 227 (2018).
[6] A. Becker, W. Lorenzen, J. Fortney, N. Nettelmann, M. Schöttler, and R. Redmer, Astrophys. J. Suppl. Ser. **215**, 21 (2014).
[7] J. Daligault and S. Gupta, Astrophys. J. **703**, 994 (2009).
[8] S. X. Hu, B. Militzer, V. N. Goncharov, and S. Skupsky, Phys. Rev. B **84**, 224109 (2011).
[9] D. Kraus, A. Ravasio, M. Gauthier, D. O. Gericke, J. Vorberger, S. Frydrych, J. Helfrich, L. B. Fletcher, G. Schaumann, B. Na-

- gler, B. Barbrel, B. Bachmann, E. J. Gamboa, E. G. S. Göde, G. Gregori, H. J. Lee, P. Neumayer, W. Schumaker, and T. D. et al., *Nat. Commun.* **7**, 10970 (2016).
- [10] D. Kraus, J. Vorberger, A. Pak, N. J. Hartley, L. B. Fletcher, S. Frydrych, E. Galtier, E. J. Gamboa, D. O. Gericke, S. H. Glenzer, E. Granados, M. J. MacDonald, A. J. MacKinnon, E. E. McBride, I. Nam, P. Neumayer, M. Roth, A. M. Saunders, A. K. Schuster, and P. S. et al., *Nat. Astron.* **1**, 606 (2017).
- [11] A. Pribram-Jones, S. Pittalis, E. Gross, and K. Burke, *Frontiers and Challenges in Warm Dense Matter*, edited by F. Graziani, et al. (Springer) (2013).
- [12] Z. Moldabekov, T. Dornheim, G. Gregori, F. Graziani, M. Bonitz, and A. Cangi, *SciPost Phys.* **12**, 62 (2022).
- [13] M. Bonitz, Z. A. Moldabekov, and T. S. Ramazanov, *Phys. Plasmas* **26**, 090601 (2019).
- [14] Z. A. Moldabekov, M. Bonitz, and T. S. Ramazanov, *Physics of Plasmas* **25**, 031903 (2018).
- [15] J. Vorberger, Z. Donko, I. M. Tkachenko, and D. O. Gericke, *Phys. Rev. Lett.* **109**, 225001 (2012).
- [16] T. S. Ramazanov, S. K. Kodanova, M. M. Nurusheva, and M. K. Issanova, *Phys. Plasmas* **28**, 092702 (2021).
- [17] D. O. Gericke, J. Vorberger, K. Wünsch, and G. Gregori, *Phys. Rev. E* **81**, 065401 (2010).
- [18] M. Lv, K. Li, C. Wang, R. Hu, Y. Zhao, and J. Dai, *Phys. Rev. E* **103**, L051203 (2021).
- [19] T. Dornheim, Z. A. Moldabekov, and P. Tolias, *Phys. Rev. B* **103**, 165102 (2021).
- [20] Z. A. Moldabekov, T. Dornheim, and M. Bonitz, *Contrib. Plasma Phys.* **62**, e202000176 (2022).
- [21] T. S. Ramazanov, S. K. Kodanova, Z. A. Moldabekov, and M. K. Issanova, *Phys. Plasmas* **20**, 112702 (2013).
- [22] M. K. Issanova, S. K. Kodanova, T. S. Ramazanov, N. K. Bastykova, Z. A. Moldabekov, and C.-V. Meister, *Laser Part. Beams* **34**, 457–466 (2016).
- [23] Z. Moldabekov, P. Ludwig, M. Bonitz, and T. Ramazanov, *Contrib. Plasma Phys.* **56**, 442 (2016).
- [24] S. K. Kodanova, T. S. Ramazanov, M. K. Issanova, G. N. Nigmatova, and Z. A. Moldabekov, *Contrib. Plasma Phys.* **55**, 271 (2015).
- [25] Z. Moldabekov, S. Groth, T. Dornheim, M. Bonitz, and T. Ramazanov, *Contrib. Plasma Phys.* **57**, 532 (2017).
- [26] S. K. Kodanova, T. S. Ramazanov, N. K. Bastykova, and Z. A. Moldabekov, *Physics of Plasmas* **22**, 063703 (2015).
- [27] Z. Moldabekov, M. Bonitz, and T. Ramazanov, *Contributions to Plasma Physics* **57**, 499 (2017).
- [28] Z. Moldabekov, T. Schoof, P. Ludwig, M. Bonitz, and T. Ramazanov, *Physics of Plasmas* **22**, 102104 (2015).
- [29] Z. A. Moldabekov, H. Kählert, T. Dornheim, S. Groth, M. Bonitz, and T. S. Ramazanov, *Phys. Rev. E* **99**, 053203 (2019).
- [30] A. L. Kritcher, A. B. Zylstra, D. A. Callahan, O. A. Hurricane, C. Weber, J. Ralph, D. T. Casey, A. Pak, K. Baker, B. Bachmann, S. Bhandarkar, J. Biener, R. Bionta, T. Braun, M. Bruhn, C. Choate, D. Clark, J. M. Di Nicola, L. Divol, T. Doeppner, V. Geppert-Kleinrath, S. Haan, J. Heebner, V. Hernandez, D. Hinkel, M. Hohenberger, H. Huang, C. Kong, S. Le Pape, D. Mariscal, E. Marley, L. Masse, K. D. Meaney, M. Millot, A. Moore, K. Newman, A. Nikroo, P. Patel, L. Pelz, N. Rice, H. Robey, J. S. Ross, M. Rubery, J. Salmonson, D. Schlossberg, S. Sepke, K. Sequoia, M. Stadermann, D. Strozzi, R. Tomasini, P. Volegov, C. Wild, S. Yang, C. Young, M. J. Edwards, O. Landen, R. Town, and M. Herrmann, *Physics of Plasmas* **28**, 072706 (2021), <https://doi.org/10.1063/5.0047841>.
- [31] O. A. Hurricane, P. T. Springer, P. K. Patel, D. A. Callahan, K. Baker, D. T. Casey, L. Divol, T. Doeppner, D. E. Hinkel, M. Hohenberger, L. F. Berzak Hopkins, C. Jarrott, A. Kritcher, S. Le Pape, S. MacLaren, L. Masse, A. Pak, J. Ralph, C. Thomas, P. Volegov, and A. Zylstra, *Physics of Plasmas* **26**, 052704 (2019), <https://doi.org/10.1063/1.5087256>.
- [32] P. Grabowski, S. Hansen, M. Murillo, L. Stanton, F. Graziani, A. Zylstra, S. Baalrud, P. Arnault, A. Baczewski, L. Benedict, C. Blancard, O. Čertík, J. Clérouin, L. Collins, S. Copeland, A. Correa, J. Dai, J. Daligault, M. Desjarlais, M. Dharma-wardana, G. Faussurier, J. Haack, T. Haxhimali, A. Hayes-Sterbenz, Y. Hou, S. Hu, D. Jensen, G. Jungman, G. Kagan, D. Kang, J. Kress, Q. Ma, M. Marciantie, E. Meyer, R. Rudd, D. Saumon, L. Shulenburger, R. Singleton, T. Sjöström, L. Stanek, C. Starrett, C. Ticknor, S. Valaitis, J. Venzke, and A. White, *High Energy Density Physics* **37**, 100905 (2020).
- [33] Z. A. Moldabekov, S. Groth, T. Dornheim, H. Kählert, M. Bonitz, and T. S. Ramazanov, *Phys. Rev. E* **98**, 023207 (2018).
- [34] D. Dubbeldam, D. C. Ford, D. E. Ellis, and R. Q. Snurr, *Molecular Simulation* **12-13**, 1084 (2009).
- [35] D. Frenkel and B. Smit, *Understanding Molecular Simulation* (Academic Press, London, 2nd ed., 2002).
- [36] D. Rapaport, *The Art of Molecular Dynamics* (Cambridge University Press, Cambridge, 2nd ed., 2004).
- [37] T. Ott and M. Bonitz, *Contributions to Plasma Physics* **49**, 760 (2009).
- [38] P. Schmidt, G. Zwicknagel, P. G. Reinhard, and C. Toepffer, *Phys. Rev. E* **56**, 7310 (1997).
- [39] H. Ohta and S. Hamaguchi, *Phys. Plasmas* **7**, 4506 (2000).
- [40] T. Saigo and S. Hamaguchi, *Phys. Plasmas* **9**, 1210 (2002).
- [41] Z. Donkó and P. Hartmann, *Phys. Rev. E* **78**, 026408 (2008).
- [42] C. Ticknor, S. D. Herring, F. Lambert, L. A. Collins, and J. D. Kress, *Phys. Rev. E* **89**, 013108 (2014).